Cement and Concrete Research 168 (2023) 107134

Contents lists available at ScienceDirect

Cement and Concrete Research

journal homepage: www.elsevier.com/locate/cemconres

Characterization of steel corrosion processes in various blended cements by means of coupled multi-electrode arrays

Miha Hren [*], Tadeja Kosec, Andraž Legat

Slovenian National Building and Civil Engineering Institute, Dimičeva ulica 12, 1000 Ljubljana, Slovenia

ARTICLE INFO

Keywords:
Blended cements
Coupled multi-electrode array
Corrosion of steel in concrete
Supplementary cementitious materials

ABSTRACT

Supplementary cementitious materials can affect the porosity of concrete, pore solution pH and chloride binding, all of which influence the type and magnitude of corrosion damage. Advanced corrosion monitoring techniques are needed to follow the development of corrosion on steel embedded in concrete across space and over time. In this study, coupled multi-electrode arrays (CMEAs) were used to characterise corrosion processes in OPC and three blended cements. Cyclic wetting with chlorides was undertaken to initiate corrosion. The results showed three distinct types of corrosion: localised corrosion (CEM I), localised corrosion that expanded over time (CEM II), and a combination of localised and general corrosion (CEM III and CEM IV). Cathodic locations were also monitored successfully, and the corrosion behaviour was related to total porosity and pH of the pore solution. MicroCT was used to quantify the volume of corroded material, which agreed well with results calculated from the CMEA measurements.

1. Introduction

Within the body of research relating to the corrosion of steel in concrete, significant attention and focus have recently been given to the steel-concrete interface [1,2], which was identified as a likely factor contributing to corrosion as early as 1975 [3]. The many features on this interface, along with concrete porosity [4], pore solution pH and chloride content [5–7], can all affect the type, size and depth of corrosion damage. For marine structures in particular, this damage can be strongly localised [8,9]. All the aforementioned factors contributing to corrosion can vary drastically according to the type of cement used. Supplementary cementitious materials (SCMs) can change the microstructure of concrete by refining the pores, lowering the pH of the pore solution, influencing the progress of carbonation and changing concrete's capacity to bind chlorides. Multiple authors have shown in their research [10–14] that the additions of slag, fly ash and natural pozzolan reduce the migration speed of chlorides towards the surface of steel. The refined pore structure is more compact, with reduced total porosity, while the ink-bottle effect can restrict the progression of chlorides [12]. Furthermore, the chloride-binding capacity of blended cements generally increases in line with the amount of clinker substituted, mainly due to the additional alumina content in the cement binder [15–17]. Since chlorides are known to initiate localised corrosion, it is expected that SCMs will influence both the rate and type of corrosion.

SCMs are also known to reduce the pH of the pore solution [18], potentially resulting in more general corrosion. Carbonation can further reduce the pH of the pore solution, which is likely the reason why carbonated concretes with increased SCM content generally have higher corrosion rates, especially under conditions of adequate humidity [19]. Even though carbonation tends to refine pores and reduce the total porosity of concrete, this does not seem to provide beneficial effects on corrosion rate reduction when SCMs are substituted in greater amounts [5]. Limited research has been conducted investigating the extent and type of corrosion damage in SCM cements, with most experiments having been conducted under the assumption that anodic corrosion activity is uniformly distributed across the exposed surface area of the working electrode, which is generally not true when chlorides are present [20,21].

Corrosion of steel in concrete is typically monitored by specialised electrochemical techniques, such as potential mapping and galvanostatic pulse (GP) [22–25], or more widely used electrochemical techniques, such as potentiodynamic polarisation and electrochemical

---

Abbreviations: CMEA, coupled multi-electrode array; WBE, wire beam electrode; EN, electrochemical noise; ER, electrical resistance; GP, galvanostatic pulse; ZRA, zero resistance ammeter; SCM, supplementary cementitious materials; OPC, ordinary Portland cement.

[*] Corresponding author.

E-mail addresses: miha.hren@zag.si (M. Hren), tadeja.kosec@zag.si (T. Kosec), andraz.legat@zag.si (A. Legat).

https://doi.org/10.1016/j.cemconres.2023.107134
Received 19 June 2022; Received in revised form 17 February 2023; Accepted 27 February 2023

impedance spectroscopy [26–30]. These techniques can be used on both existing structures and laboratory specimens, as long as there is electrical contact to the rebars and physical access to the concrete surface. The downside of these techniques is, however, the limited information they provide regarding spatial corrosion. It is possible to control the location of the measurement to a certain extent by placing the measuring probe (counter electrode) at different locations across the concrete surface. The surface area covered by the probe still polarizes a relatively large chunk of metal, which averages-out information on localised corrosion. Some research has been conducted in an attempt to adapt these methods in order to detect localised corrosion [31], but while such a method improves the accuracy of the corrosion rates measured, it doesn't provide additional spatial information about the corrosion processes.

Embedded sensors are seldom used for monitoring, as they need to be embedded in concrete before casting [32,33]. When used, however, they can provide additional spatial information about corrosion. Electrical resistance (ER) sensors are a physical sensoring solution which can be used to directly calculate a reduction in the thickness of steel by analysing changes in measurements of the steel's resistance [34,35]. Such sensors can provide continuous monitoring of corrosion at locations they are placed, but they are only sensitive to anodic corrosion activity. Similar to the conventional methods mentioned previously, localised corrosion can only be partially detected, as the corrosion activity is averaged across the entire exposed surface of the sensor electrode. A more advanced method for monitoring corrosion is the coupled multi-electrode array (CMEA) technique [35,36]. CMEAs use a grid of multiple steel electrodes, with each electrode in the array coupled to the other electrodes through an ammeter. Both anodic and cathodic corrosion currents can therefore be measured, with the electrodes acting as a single coupled steel surface. CMEAs are often used to monitor localised corrosion phenomena, such as crevice corrosion or pitting corrosion [37–42], and in situations where the type of corrosion is unknown [43–46]. Despite this, however, they are rarely used in concrete applications [35,47], even though steel in concrete can exhibit pronounced localised corrosion [5,8].

The research conducted in this study was a continuation of our previous study [5], where the same cement mortars were analysed both in terms of their microstructural properties and corrosion performance using ER sensors and galvanostatic pulse technique. The results showed that cements with higher degree of cement clinker (CEM I and CEM II) were subjected to more localised corrosion, which was tied to the lower total porosity, higher amount of larger capillary pores, as well as higher pH value of the pore solution. The opposite was true for cements with larger amount of SCMs (CEM III and CEM IV), where a higher degree of general corrosion was observed, likely due to better pore refinement and a decrease in pH value. This effect was even more pronounced for blended cements in carbonated mortars. The study also showed that most of these observed differences started showing between 15 and 30 weeks after chloride exposure, and were the most pronounced beyond week 30. For the first 15 weeks of exposure, little differences were observed between cements, with only CEM III showing increased corrosion activity. The limitations of the ER and GP techniques in detecting both early corrosion and the transition from initiation to propagation stage prompted us to conduct further studies using a more advanced CMEA technique within that time frame.

The goal of this study was to implement the CMEA technique to monitor the corrosion of steel in mortars made of various blended cements, in which varying degrees of corrosion localisation were expected. Corrosion in OPC, slag, fly ash and limestone cement mortars was monitored for at least 14 weeks, and cyclic wetting and drying with chlorides was used to initiate corrosion. Special emphasis was placed on the timing and location of the appearance of anodic and cathodic locations, the extent of the area covered, the size of the corrosion current densities, and the distribution of corrosion damage over time. CMEA results were also verified with X-ray computed microtomography, where the corrosion damage determined from the measured anodic currents was compared to that obtained from quantitative microCT analysis of volume loss. The results were tied and compared to our previous research on the same cements using various other corrosion techniques [5,48].

2. Materials and methods

2.1. Specimen preparation

A total of 4 CMEA specimens were prepared for the corrosion monitoring experiments, one for each type of cement used. CMEA specimens consisted of 25 steel electrodes arranged in a 5 × 5 array, which were covered with epoxy resin and placed in a 3D printed housing. These specimens needed to be suitable for CMEA corrosion measurements, as well as small and compact enough to be examined by computed microtomography (microCT). To meet these needs, custom-made specimens were designed using a 3D printer, epoxy filler, steel wire rods and connectors. The finished CMEA specimen is shown in Fig. 2b. First a framework was designed in a 3D CAD program and then 3D printed. In the second phase, wires of 0.5 mm diameter were inserted into the frame and protected with epoxy resin. The exposed area of the wire cross-section was ground with sandpaper (up to 2500-grit) and the electrodes were degreased with acetone. In the final phase, a pool 5 mm deep was made for casting the mortar.

2.2. Preparation of the cements and mortar

Mortars used in this research were prepared using ordinary Portland cement (OPC) as reference cement, and three other commercially available blended cements, all made with the same cement clinker. The cements were in accordance with the standard EN 197-1:2011 [49] and had the following designations:

- CEM I 42.5 N (OPC),
- CEM II/B-M (LL-V) 42.5 N (fly ash and limestone),
- CEM III/B (S) 32.5 N – LH/SR (blast-furnace slag),
- CEM IV/A (V-P) 42.5 R SR (fly ash and natural pozzolan).

Throughout the paper, the cements will be referred to by their shorthand designations: CEM I, CEM II, CEM III and CEM IV, respectively.

A water-to-binder ratio of 0.75 and a cement-to-aggregate ratio of 0.33 were used to prepare mortars from each of the cements. Additionally, the aggregate used in the standard for determining the strength of cements [50] was sieved to ensure a maximum aggregate size of 1 mm. These two measures were taken to increase the porosity of the mortar and speed up the corrosion processes, as well as to accommodate the small diameter of the CMEA electrodes and the shallow depth of cover (5 mm).

The mortar mixes were placed inside the pool on top of the CMEA specimens (Fig. 2d) and a vibration table was used to consolidate the mortars and achieve the same cover depth (of 5 mm) for all the specimens. The mortars were then cured at 20 ± 2 °C and 100 % relative humidity for 28 days before any other corrosion-initiating exposure was introduced.

Total porosity, free chloride concentration, pH value and pore size distribution were determined for each cement mortar in our previous research [5,48]. The measurements were done at different periods during the 52-week chloride exposure. The properties relevant for this study are shown in Table 1 and in Fig. 1.

2.3. Exposure

After the 28-day curing period, chloride ions were introduced through cyclic ponding with a 3.5 % NaCl solution. A 3D printed pool

Table 1
Total porosity [volume %] of mortars measured after 47 weeks of chloride exposure, free chloride concentration [g/L] and pH of the extracted pore solutions measured after 35 weeks of chloride exposure.

Mortar	CEM I	CEM II	CEM III	CEM IV
Total porosity [volume %]	16.1	18.6	19.6	17.1
Chloride content [g/L]	61.0	84.9	48.0	74.9
pH	12.05	11.81	11.45	12.06

was placed on the upper side of the specimens to keep the solution on the exposed part of the mortar. Weekly cycles consisted of 3 days wetting followed by 4 days drying. At the start of the drying period, any remaining solution in the pool was absorbed with a pipette to accelerate the drying process. Each specimen was exposed to 14 wet-dry cycles, totalling 14 weeks of exposure.

2.4. Corrosion monitoring

Corrosion was continuously monitored throughout the 14 weeks of exposure using custom-made Zero Resistance Ammeters (ZRAs). ZRAs consisted of 25 individual ammeters, coupled together through the steel electrodes on one end, and a common floating ground on the other. Together, these components formed the CMEA monitoring system. Fig. 2a shows a schematic representation of the CMEA system, including an image of a specimen containing mortar (Fig. 2d). As the various coupled steel electrodes form anodic and cathodic sites, positive or negative corrosion current flows through both them and the individual ZRAs. Each current recorded thus represents the sum of all anodic and cathodic current flowing through a certain electrode. In the present ZRA system, positive currents represent anodic currents while negative currents represent cathodic currents. More details on how similar ZRA systems have been implemented by other authors for CMEA or electrochemical noise measurements can be found in [36,39].

Each mortar specimen was measured at a rate of 1 Hz. The minimum and maximum measurable current was ±5 μA, with a resolution of 150 pA per electrode. Given the electrode diameter of 0.5 mm, this roughly translated to a maximum measurable current density of ±2.5 mA/cm2, with a resolution of 76 nA/cm^2. Eq. (1) [51] was used to calculate the corrosion rate (v_{corr} in μm/year) from the corrosion current density (j_{corr} in μA/cm^2), with the following values used for constants: molar mass $M = 55.845$ g/mol, oxidation number $z = 2$, density $\rho = 7.85$ g/cm^3 and a constant of 3.27 in μm g/μA cm year, obtained from Faradays Law.

$$v_{corr} = \frac{3.27M}{z\,\rho} j_{corr} \tag{1}$$

Another assumption in the corrosion rate calculations was that the corrosion damage was equally distributed along the entire cross-section of each electrode. In order to obtain results more comparable to the microCT results, corrosion damage at the end of exposure was also calculated according to the reduction in volume of each electrode, by integrating the corrosion current over time and using a modified version of Eq. (1).

2.5. Post-exposure validation

At the end of the chloride exposure, the specimens were non-destructively examined using an Xradia MicroXCT-400 microCT scanner. Sections of the CMEA electrodes were scanned at 150 kV and 10 W, using a macro objective with 0.71× magnification. A High Energy #1

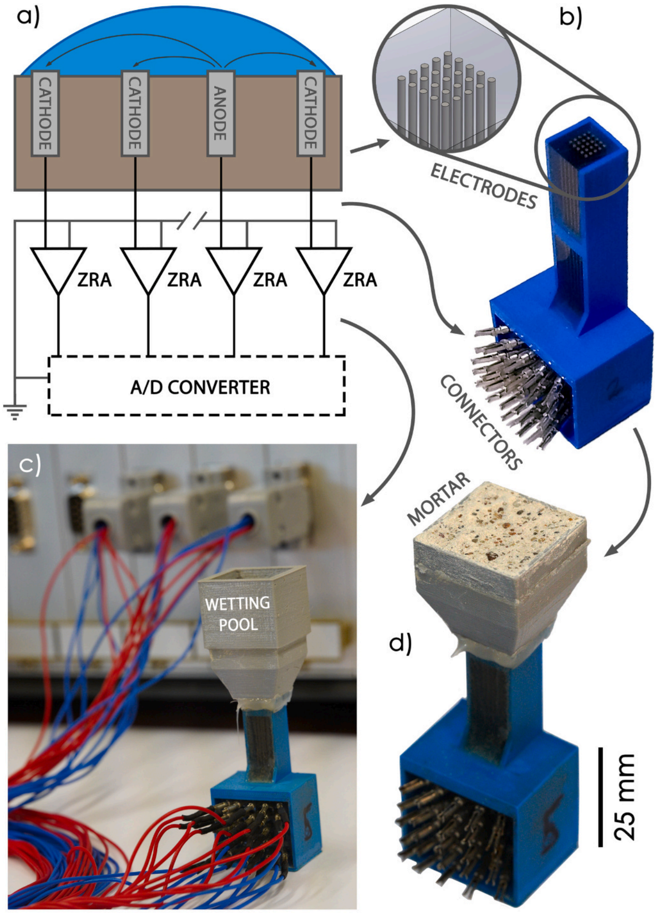

Fig. 2. Overview of the CMEA principle of operation: (a) Schematic view, (b) specimen with visible electrodes, (c) specimen connected by cables to the ZRA device (in the background) and (d) specimen with visible mortar.

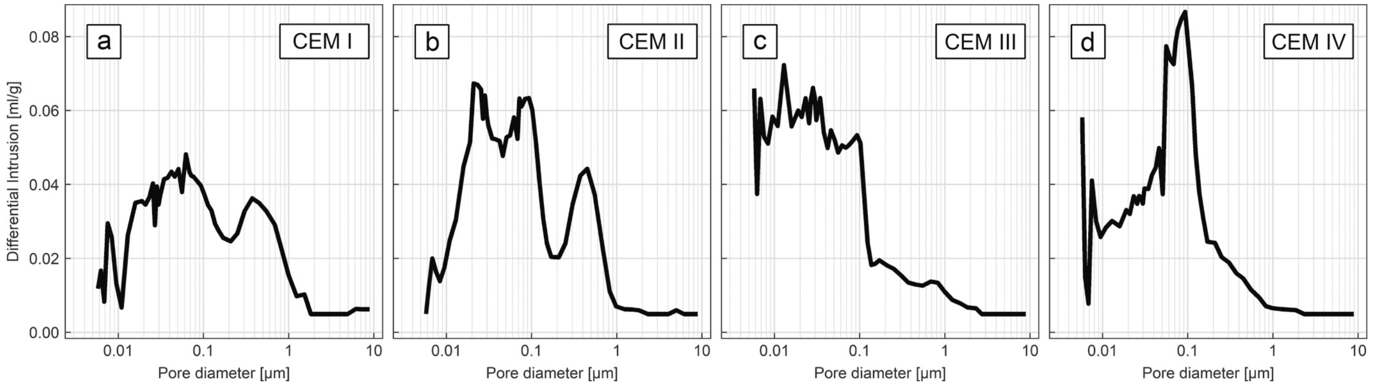

Fig. 1. Pore size distribution for (a) CEM I, (b) CEM II, (c) CEM III and (d) CEM IV mortars after 47 weeks of chloride exposure.

filter was used, and the scan required 4 h for each specimen. The resolution obtained was 7 μm per voxel.

3D images were analysed using Avizo Inspect 2019.1 software. In order to calculate the corroded volume for each electrode, the volumes of the damaged electrodes were first measured using threshold segmentation and label volume analysis. Since the electrodes were in the shape of a straight cylinder, the original volume of each was calculated from height and cross-section measurements of the scanned electrode. The cross-sectional area was obtained by measuring the volume of an undamaged part of an electrode and dividing it by its height. In this way, the cross-sectional area represented the average value, as there was some variation in dimensions across the length of the electrode. Finally, the corroded volume was calculated as the difference between the original volume of the undamaged electrode and its volume following the damage.

3. Results

3.1. Distribution of corrosion and its propagation over time

Corrosion currents on 4 mortar specimens, made from CEM I, CEM II, CEM III and CEM IV cements, were monitored for 14 weeks using the CMEA technique. Results of the average anodic and cathodic corrosion current densities are summarized in Fig. 3. The results are shown in array form, with the red dots representing electrodes that were predominantly anodic, and the green dots those that were predominantly cathodic. Where electrodes were both anodic and cathodic in a single week, the anodic reaction is prioritized. The light grey dots indicate that no corrosion activity occurred on the electrode. The intensity of the colours is presented in a logarithmic scale, as multiple orders of magnitude exist between the passive and active corrosion current densities. The rows (1 to 5) and columns (A to E) of each array of electrodes are labelled. The same label nomenclature will be used throughout this

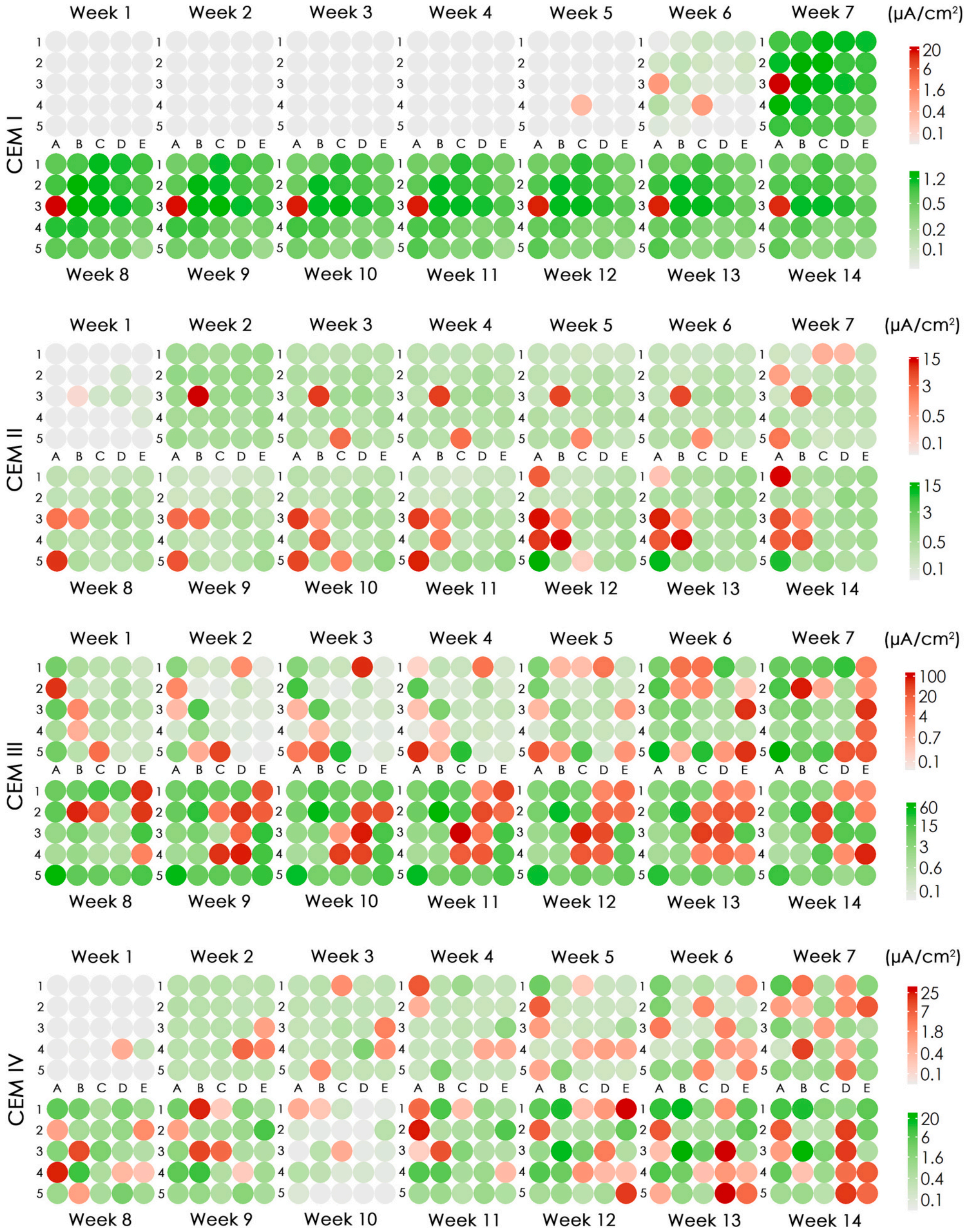

Fig. 3. Average corrosion current densities showing the anodic (red) and cathodic (green) reactions for the CEM I, CEM II, CEM III and CEM IV cements, represented in array form. (For interpretation of the references to colour in this figure legend, the reader is referred to the web version of this article.)

article in order to describe particular electrodes of any given array.

The results represented in Fig. 3 show 3 distinct types of corrosion behaviour. The first type is an extremely localised corrosion that only develops after 6 weeks of exposure, with only a single anodic location, as was observed in the case of cement CEM I. The second type of corrosion behaviour was observed on the CEM II cement, where localised corrosion developed early on, but over time the anodic location started to expand to nearby electrodes. The third type of behaviour, observed on both CEM III and CEM IV cements, was a combination of localised and general corrosion, where anodic locations are distributed across multiple electrodes, but certain electrodes still stand out as more anodic than others. Each of these distinct types of corrosion will be looked at in more detail in the following paragraphs.

As mentioned previously, in Fig. 3 the CEM I specimen shows predominantly localised corrosion on a single electrode. Fig. 4 gives a more continuous insight into the cathodic and anodic behaviour of individual electrodes over time. Anodic corrosion currents are displayed as positive, while cathodic corrosion currents are displayed as negative. The sum of all anodic and cathodic currents at any given time was zero. The curves are colour-coded, as detailed in the top left array in Fig. 4, and its rows and columns are labelled, as defined previously. The blue areas in the background represent the wetting cycles, which started at the beginning of each week and lasted for 3 days. For the first 5 weeks, no corrosion activity was detected, with the first anodic peak recorded only at the start of the 6th wetting period. This occurred on electrode C4, with a proportionate cathodic response from all other electrodes. All currents returned to zero within 12 h, indicating that the electrode had returned to a passive state. Roughly 2 days after the end of the 6th wetting period, another electrode (A3) became anodic. This time, the electrode did not return to its passive state, and the corrosion process was continuously initiated at the start of each wetting period until the end of the exposure (cycles 7–14). The corrosion rates attained during these wetting periods reached values of over 800 μm/year, but only for very short periods of time. Generally, the corrosion rates on the A3 electrode wavered between 200 and 500 μm/year. While all other electrodes contributed to the cathodic reaction, electrodes in the immediate vicinity of the A3 electrode (e.g. B2, B3, B4 and C3) experienced slightly higher cathodic currents compared to those further away (e.g. the electrodes in column E).

Fig. 5 represents the anodic and cathodic currents over time for the CEM II specimen. In order to make the graph clearer, currents are only displayed for the electrodes that underwent significant corrosion activity, while the rest are hidden. The electrodes hidden in Fig. 5 are coloured white in the array on the bottom left. The B3 electrode was the first to have significant anodic activity, which started in the 2nd wetting cycle. Over the next 6 wetting cycles, the B3 electrode slowly transitioned towards both anodic and cathodic behaviour, with corrosion rates of around 200 μm/year. During the same period, the C5 electrode also exhibited anodic activity (at a rate of over 1000 μm/year), but only for around 12-hour intervals at the beginning of each wetting cycle. All other electrodes contributed relatively equally to the cathodic reaction. After the 6th wetting cycle, corrosion processes started on several other neighbouring electrodes. Electrodes A3 and A5 showed large anodic peaks (equivalent to rates of above 1000 μm/year) at the beginning of the wetting cycles, while the latter also seemed to interchange between anodic and cathodic at the beginning of the drying periods. During the final 3 weeks of exposure, electrodes B4, A4 and A1 also began to contribute towards the total anodic current, indicating that corrosion behaviour became less localised over time.

The results of anodic and cathodic corrosion currents for the CEM III specimen are shown in Fig. 6. Since almost all the electrodes contributed to the corrosion exchange, none were hidden from display, but specific electrodes were labelled in order to emphasize their importance. Corrosion activity was detected on multiple electrodes from the very 1st wetting cycle onwards. While at the start of the wetting periods corrosion rates reached very high values (up to 8000 μm/year), during the first 10 weeks of exposure the bulk of corrosion damage occurred during the drying periods. With the exception of the 5th cycle, for the first 10 weeks a different electrode became anodic during each consecutive drying period. The following electrodes became anodic, in the order given: A2, C5, D1, A5, E5, E3, E1 and D4. These electrodes are positioned completely separately from one another, as can be seen in Fig. 3 (in the CEM III row), with unconnected electrodes exhibiting corrosion damage at the end of each consecutive week. Such behaviour is typical for general corrosion, in which, over a sufficient period of time, the entire steel surface would be corroded to a roughly similar extent. The corrosion rates of the electrodes mentioned generally remained below 4000 μm/year, reducing to zero within 2 days of the start of the drying period. Observation of the results after week 10, however, showed that the anodic location stabilized on electrode C3, indicating the start of more localised corrosion. This electrode showed similar corrosion behaviour to other electrodes, peaking at the start of the wetting and drying periods, and then reducing close to zero within 2 days of the start of the drying period. Throughout the exposure the cathodic reaction was concentrated on the D3, D5, A5 and B2 electrodes, but other electrodes also contributed to a lesser degree.

The results of anodic and cathodic corrosion activity for the CEM IV specimen are presented in Fig. 7. Results from the 10th wetting cycle are missing due to technical issues, but the currents were still measured during this period. As previously, all electrodes are displayed, as most of them contributed to the anodic-cathodic current exchange. Although corrosion processes were detected within the 1st week of exposure, the

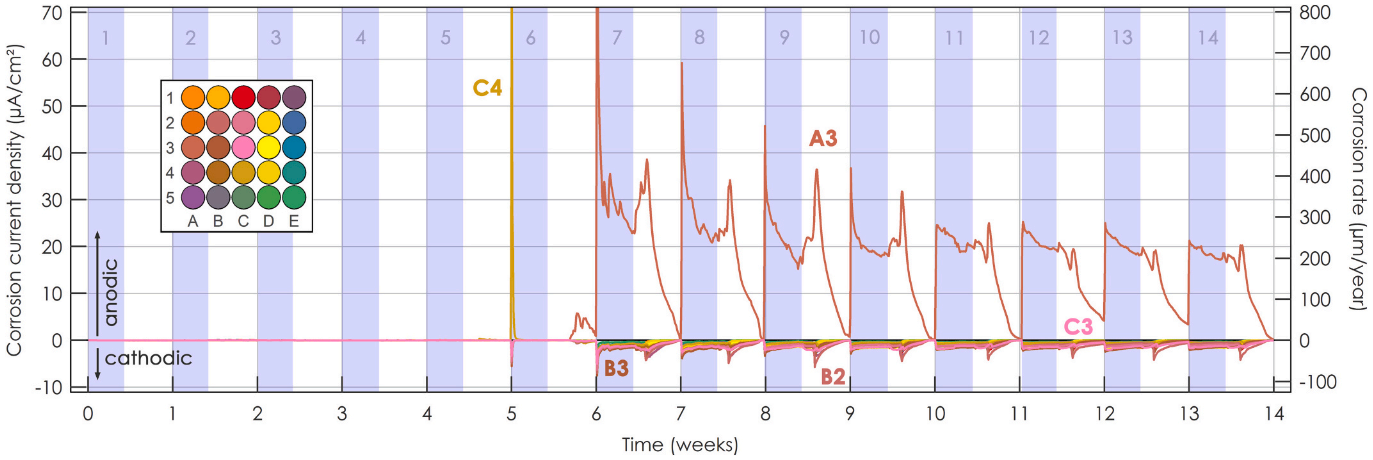

Fig. 4. Anodic and cathodic currents for the CEM I specimen over 14 weeks of exposure to cyclic wetting and drying.

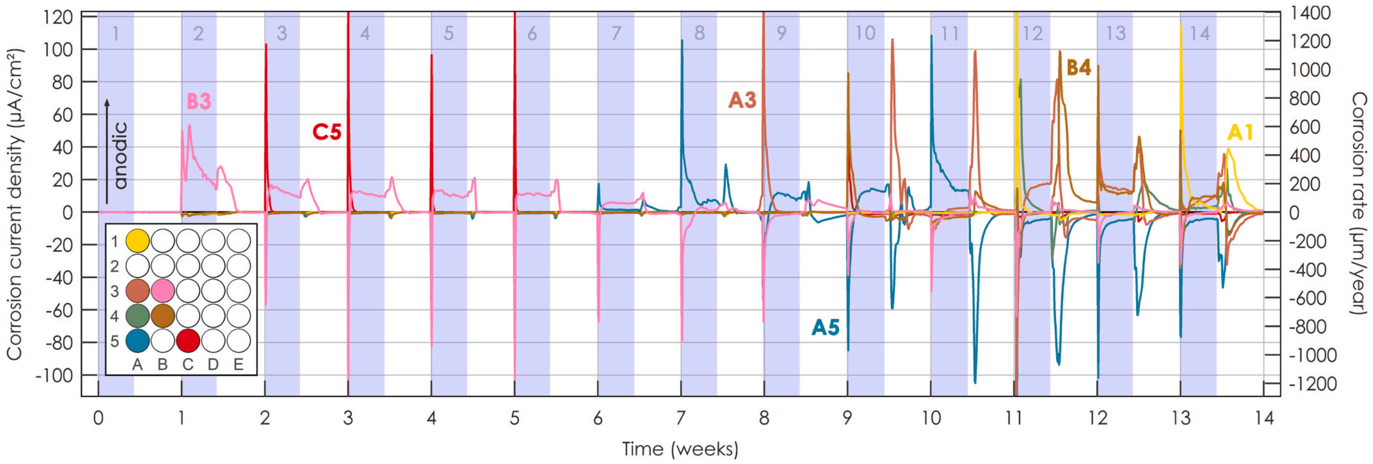

Fig. 5. Anodic and cathodic currents for the CEM II specimen over 14 weeks of exposure to cyclic wetting and drying. Only electrodes that had significant corrosion activity are displayed.

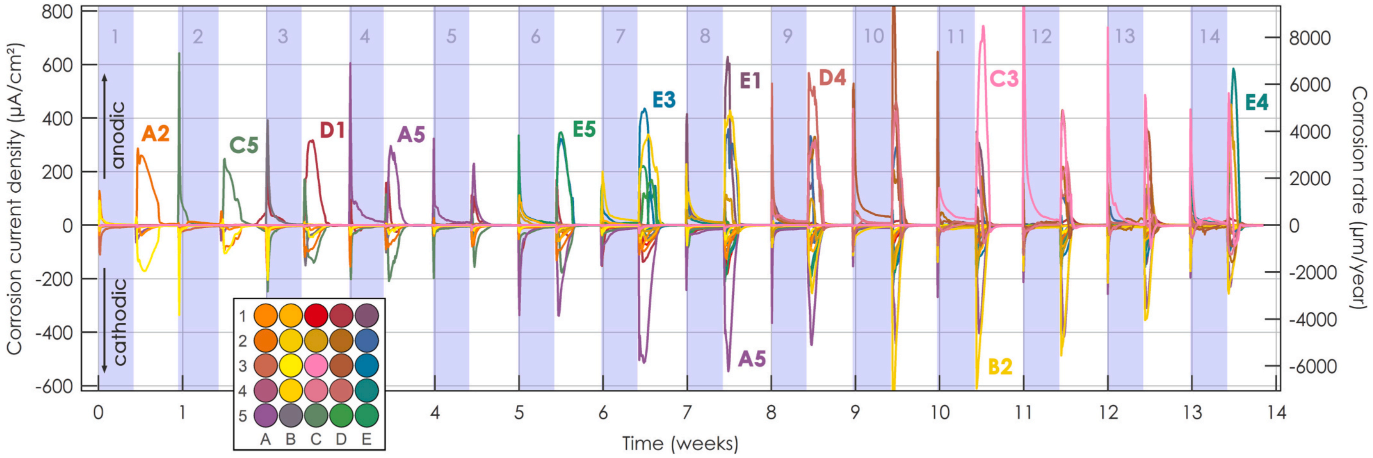

Fig. 6. Anodic and cathodic currents for the CEM III specimen over 14 weeks of exposure to cyclic wetting and drying.

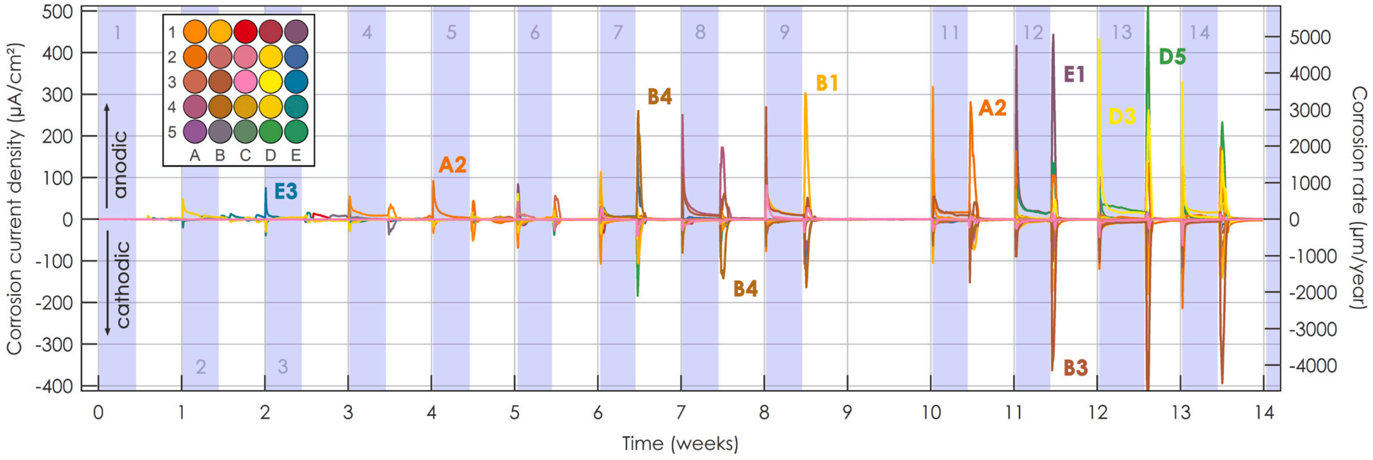

Fig. 7. Anodic and cathodic currents for the CEM IV specimen over 14 weeks of exposure to cyclic wetting and drying.

magnitude of corrosion activity during the first 6 weeks was relatively low compared to the remainder of the exposure period. Electrodes E3 and A2 showed increased amount of anodic activity, while the latter also contributed towards the cathodic current. Corrosion rates did not surpass 1000 μm/year, and remained below 500 μm/year throughout most of the initial 6 weeks of exposure. Starting at week 7, however, the corrosion activity started to significantly increase. Electrodes B4, B1, A2, E1 D3 and D5 started to become anodic, in the order given, but unlike in the CEM III specimen, they contributed towards the anodic current for multiple consecutive wetting cycles, before then becoming less active

(Fig. 3). Three electrodes in particular (A2, D3 and D5) were the most anodic in the end, with most of the corrosion damage occurring within the final 4 weeks. This indicated the occurrence of more localised corrosion behaviour on these electrodes, as can also be observed in Fig. 3 (row CEM IV). All the anodic electrodes previously listed displayed corrosion rates of above 3000 μm/year at the start of the wetting/drying periods, which were generally reduced to below 1000 μm/year within 24 h.

Before week 7, most of the cathodic activity on the CEM IV specimen was distributed fairly evenly across all the electrodes, while after that, the majority of activity occurred on electrodes B2, B3 and B4. In at least 1 cycle prior, these electrodes were predominantly anodic, and as the anodic currents became more localised on individual electrodes, so did the cathodic currents.

3.2. *Current changes in the wetting and drying cycles*

Up until now, only changes across the entire period of exposure have been analysed and discussed. CMEA, however, can also be used to assess detailed corrosion activity over shorter periods of time. Fig. 8 shows the corrosion current densities and corrosion rates over one week of exposure. Week 12 was chosen for all cement types, with the figures labelled in sequence from (a) to (d) for cements CEM I to CEM IV, respectively.

Fig. 8a shows the corrosion current results for the CEM I specimen in week 12. This represented the simplest current response, in which one electrode (A3) became anodic, while all other electrodes became cathodic. The anodic response appeared very soon after the start of the wetting cycle, then slowly started to decrease during wetting. About 3 h after the start of the drying period, the anodic current slightly increased, before decreasing rapidly during the drying period. The A3 electrode did not return to a zero current before the next wetting cycle began, indicating that it did not completely dry during the drying period.

Fig. 8b shows week 12 of the corrosion current results for the CEM II specimen. The results were more complex than for the CEM I specimen, with multiple electrodes transitioning from an anodic to cathodic corrosion current. Electrodes A1 and A4, for example, were both extremely anodic during the wetting period, but their behaviour transitioned to cathodic as the drying period commenced. The currents of electrodes B4 and A3, on the other hand, had already transitioned from cathodic to anodic during the wetting cycle, and then exhibited the most anodic behaviour during the drying period, reaching corrosion rates of around 1000 μm/year. It is also worth noting that, during the drying period, the corrosion activity on electrodes B4, A3 and A5 seem to be interconnected, as when the current of one of these electrodes changes over time, the other two electrodes exhibit a proportional and inverse response.

Fig. 8c shows week 12 of the corrosion current results for the CEM III specimen. This represents a typical response observed on the CEM III specimen over multiple wetting cycles, where a small number of electrodes displayed an initial spike at the start of the wetting period, while the majority of electrodes responded with a proportional cathodic reaction. After the initial spike, all currents slowly converged towards

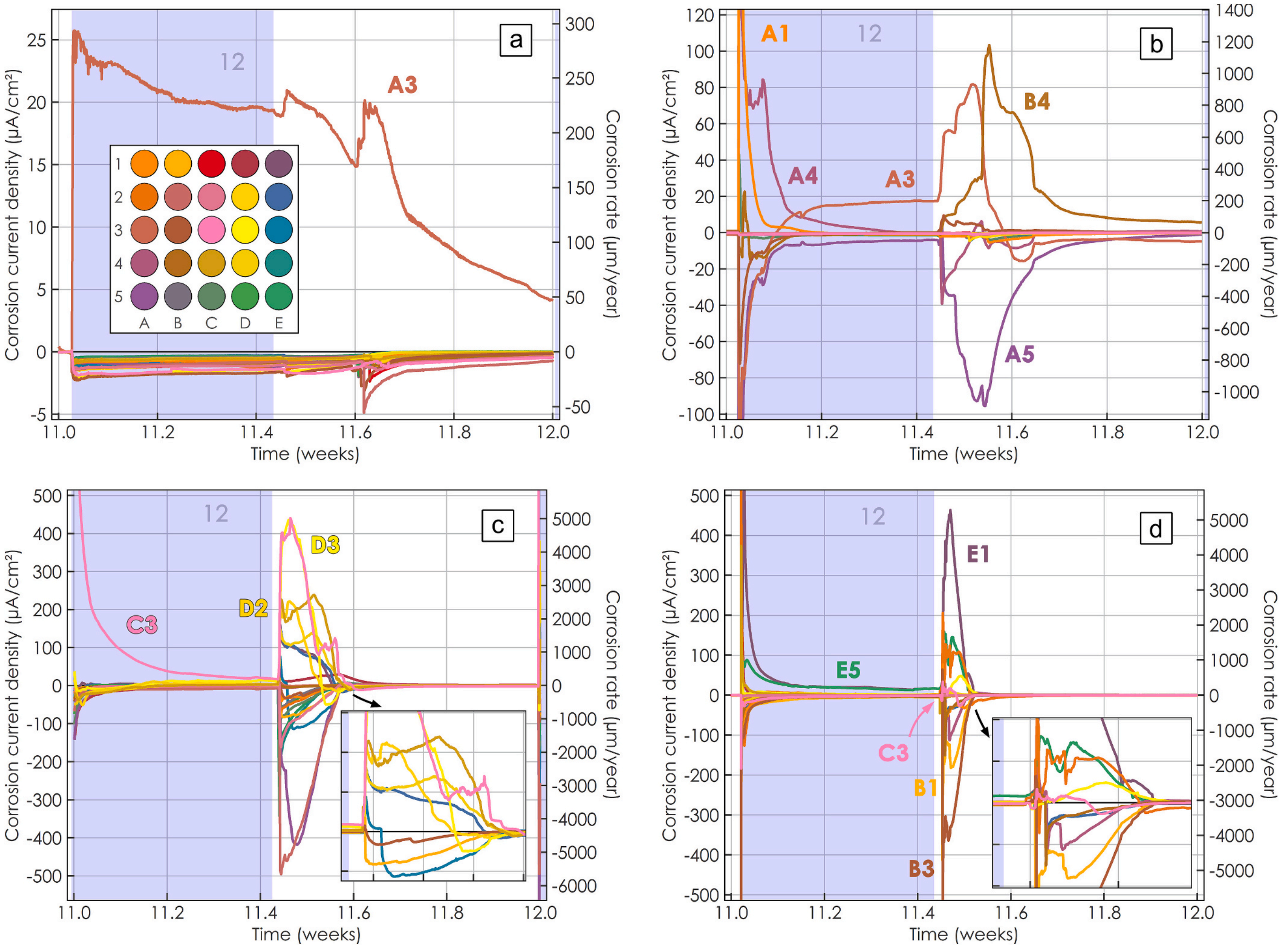

Fig. 8. Anodic and cathodic currents in the (a) CEM I specimen, (b) CEM II specimen, (c) CEM III specimen and (d) CEM IV specimen during the 12th week of exposure. CEM III and CEM IV specimens also include detailed view of the drying period with selected electrodes visible.

zero, then increased again about 3 h after the start of the drying period. During these cycles, most electrodes are either anodic or cathodic, but they rarely transition between the two states. Fig. 8c shows that electrodes D2 and D3 were anodic during both wetting and drying cycles, while multiple other electrodes became either anodic or cathodic after the drying period started, reaching corrosion rates of up to 5000 μm/year. All currents returned to zero before the next wetting cycle started, indicating that the specimen completely dried during the drying period.

Fig. 8d shows week 12 of the corrosion current results for the CEM IV specimen. The corrosion behaviour was very similar to the CEM III mortar, which exhibited an initial anodic spike during the wetting cycles that slowly converged towards zero. As the drying period started, there was a rapid increase in both the cathodic and anodic currents, with only the C3 electrode transitioning its current from anodic to cathodic within the same drying cycle. Most of the anodic activity occurred on electrodes E5 and E1, where corrosion rates were as high as 5000 μm/year, while most cathodic activity occurred on electrodes B1 and B3.

3.3. Average and local corrosion rates

When using conventional electrochemical techniques, it is common to measure certain parameters (e.g. current, potential, impedance and polarisation resistance) and then apply results to the entire exposed surface of the working electrode. Since there is usually no prior information regarding the size of the anodic portion of the surface area exposed, or this area is inaccessible behind a layer of concrete, this is a reasonable assumption to make. The same principle can be applied to CMEA measurements, with the goal of getting results comparable to those that conventional electrochemical techniques would measure on the same corrosion system. Fig. 9a shows the average corrosion current densities calculated in such a manner. For each week of exposure, the total anodic current was divided by the total surface area across all 25 electrodes, regardless of whether or not they were anodic or cathodic during that week. The corrosion current densities and corrosion rates obtained in this way will therefore be either lower or equal to the corrosion rates calculated on individual electrodes, depending on the degree of localised corrosion.

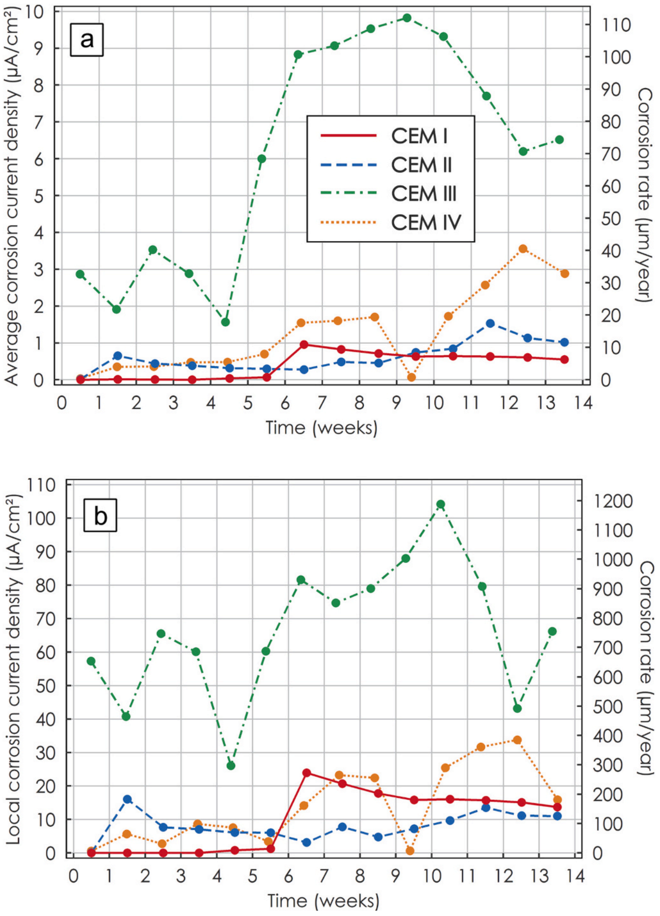

Fig. 9. (a) Average corrosion current densities, obtained by applying the total anodic current across all 25 electrodes; (b) highest local corrosion current densities.

The results in Fig. 9a show that, during the first 6 weeks of exposure, the CEM I specimen underwent the least amount of anodic activity, while the CEM III specimen exhibited the highest average corrosion rates, with the CEM II and CEM IV specimens lying in between. After the 6th week, the CEM I specimen exhibited a larger increase in corrosion rate, but it never exceeded 10 μm/year, and started to decrease as the exposure continued. At the same time, the average corrosion rates of both the CEM II and CEM IV specimens increased over time, respectively surpassing 10 and 30 μm/year by the end of the exposure period. The CEM III specimen had the highest average corrosion rates over the entire period of exposure, showing a general upward trend over time.

In contrast to the average corrosion rates presented in Fig. 9a, the highest local corrosion rates for each week are plotted in Fig. 9b. These data points were obtained by taking the most anodic electrode for any given week, and calculating its average corrosion rate for the same week. As can be seen by the scale on the y-axis, localised corrosion rates are about one order of magnitude higher that the average corrosion rates. Although, in terms of corrosion rates, the mortars are in the same order at the beginning, the CEM I and CEM II specimens switch places with respect to corrosion after week 6, as corrosion on the CEM I specimen becomes significantly more localised. The other 3 specimens follow similar trends, as observed in the previous paragraph.

3.4. Post-exposure validation

At the end of the 14 week period of chloride exposure, non-destructive post-exposure analysis was conducted on all 4 CMEA specimens using a microCT scanner, the results of which are presented in Fig. 10. The column on the left shows the volume of corrosion damage calculated using the CMEA technique at the end of the period of chloride exposure. These volumes were calculated by integrating the corrosion current of each electrode over time, and using a slightly modified version of Eq. (1) to calculate the volume. The column on the right represents the volumes obtained using the CT technique, by calculating the difference in volume between the electrodes initially and after corrosion damage occurred. The middle column shows a visual representation of the corrosion damage according to microCT evaluation.

The volumes of the CEM I and CEM II specimens were generally in good agreement between the two methods. All the anodic electrodes were identified correctly, corrosion damage was identified at the same order of magnitude, and results agreed with the visible damage to the electrodes. In both specimens CT volumes below 1.0×10^6 μm^3 were measured in multiple electrodes, but both visual representation and calculations of the CMEA volumes did not, however, show any damage to these electrodes. This is likely, because there is some margin of error when subtracting the volume of the original electrode from its damaged CT volume, due to irregularities arising along the length of the electrode. With the exception of the A3 (CEM I) and B3 (CEM II) electrodes, where corrosion was present along the length of the electrode, most electrodes were damaged across the exposed surface of their cross-section.

Generally, the CMEA and CT volumes were also in good agreement for the CEM III specimen, except in the case of the C4 and E2 electrodes, where the scanned CT volumes were twice the size as those obtained by the CMEA technique. As previously, the volumes calculated by both techniques related well to the damage assessed visually, which predominantly occurred on the exposed cross-sections of the electrodes, as opposed to the epoxy-covered sides. It's also worth pointing out that the

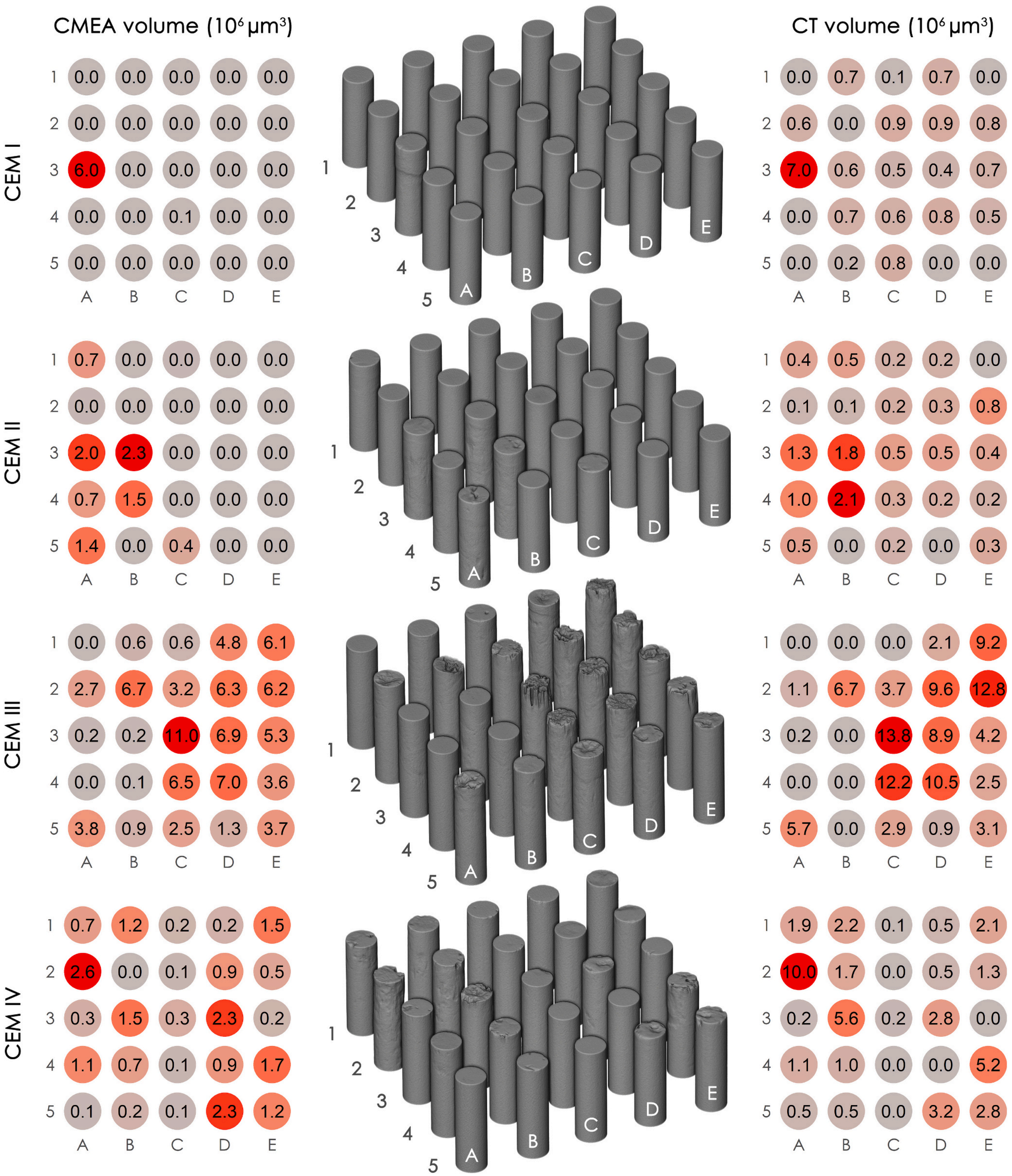

CMEA volume (10^6 μm^3)

CT volume (10^6 μm^3)

CEM I

	A	B	C	D	E
1	0.0	0.0	0.0	0.0	0.0
2	0.0	0.0	0.0	0.0	0.0
3	6.0	0.0	0.0	0.0	0.0
4	0.0	0.0	0.1	0.0	0.0
5	0.0	0.0	0.0	0.0	0.0

	A	B	C	D	E
1	0.0	0.7	0.1	0.7	0.0
2	0.6	0.0	0.9	0.9	0.8
3	7.0	0.6	0.5	0.4	0.7
4	0.0	0.7	0.6	0.8	0.5
5	0.0	0.2	0.8	0.0	0.0

CEM II

	A	B	C	D	E
1	0.7	0.0	0.0	0.0	0.0
2	0.0	0.0	0.0	0.0	0.0
3	2.0	2.3	0.0	0.0	0.0
4	0.7	1.5	0.0	0.0	0.0
5	1.4	0.0	0.4	0.0	0.0

	A	B	C	D	E
1	0.4	0.5	0.2	0.2	0.0
2	0.1	0.1	0.2	0.3	0.8
3	1.3	1.8	0.5	0.5	0.4
4	1.0	2.1	0.3	0.2	0.2
5	0.5	0.0	0.2	0.0	0.3

CEM III

	A	B	C	D	E
1	0.0	0.6	0.6	4.8	6.1
2	2.7	6.7	3.2	6.3	6.2
3	0.2	0.2	11.0	6.9	5.3
4	0.0	0.1	6.5	7.0	3.6
5	3.8	0.9	2.5	1.3	3.7

	A	B	C	D	E
1	0.0	0.0	0.0	2.1	9.2
2	1.1	6.7	3.7	9.6	12.8
3	0.2	0.0	13.8	8.9	4.2
4	0.0	0.0	12.2	10.5	2.5
5	5.7	0.0	2.9	0.9	3.1

CEM IV

	A	B	C	D	E
1	0.7	1.2	0.2	0.2	1.5
2	2.6	0.0	0.1	0.9	0.5
3	0.3	1.5	0.3	2.3	0.2
4	1.1	0.7	0.1	0.9	1.7
5	0.1	0.2	0.1	2.3	1.2

	A	B	C	D	E
1	1.9	2.2	0.1	0.5	2.1
2	10.0	1.7	0.0	0.5	1.3
3	0.2	5.6	0.2	2.8	0.0
4	1.1	1.0	0.0	0.0	5.2
5	0.5	0.5	0.0	3.2	2.8

Fig. 10. The volume of corrosion damage measured using the CMEA technique (left) compared to that evaluated using the microCT scanner (right). Middle column shows volumetric visual representation of corrosion damage obtained using microCT.

corrosion damage on each electrode was not evenly distributed across its cross-section, which can have negative ramifications on the calculated corrosion rates analysed in previous chapters.

The largest discrepancy between the volumes obtained using the CT and CMEA methods occurred in the CEM IV specimen. Electrodes A2, B2, B3 and E4 show 3 to 5 times higher corrosion damage when using the CT technique compared to that calculated using CMEA. While most corrosion damage was present on the cross-sections of the electrodes, some side damage was visible on electrodes A2 and B2. Electrode B2 was also visibly damaged, but no anodic corrosion activity was detected using the CMEA technique.

4. Discussion

The corrosion processes in mortars made of CEM I, CEM II, CEM III and CEM IV cements were characterised by the combined use of the Coupled Multi Electrode Array (CMEA) technique and microCT. It was expected that the CMEA technique would make it possible to follow the spatiotemporal behaviour of individual corrosion processes, including the assessment of local corrosion rates over time. In our previous study [5], the mortar microstructure and general corrosion properties of similar, non-carbonated and carbonated mortars were investigated by means of the galvanostatic pulse (GP) technique and electrical resistance (ER) probes. Specific outcomes related to localised corrosion were confirmed by CT scans of embedded rebars. The main aim of the present research was to understand the time evolution of corrosion processes during the first 14 weeks of exposure in non-carbonated blended cements contaminated by chlorides, with an emphasis on the localization of these processes.

The study of steel corrosion in cement CEM I showed that only a single electrode became anodic, staying in such condition for the rest of the exposure, indicating that corrosion was mostly localised. Such corrosion performance was attributed to a higher pH, lower porosity (Table 1) and higher number of larger capillary pores (>0.1 μm, Fig. 1), all of which were determined on the same cements in our previous study [5,6]. Observations related to porosity are also in accordance with studies done by other authors regarding porous materials [4]. Cathodic reactions were equally distributed across all other electrodes, with the electrodes located closer to the anodic location having a slightly higher corrosion density compared to those further away. This was expected, as it has been shown previously that cathodic currents decrease in line with the distance from an anodic location, most likely due to an increasing resistivity in concrete [52,53]. A different type of corrosion behaviour was observed in CEM II, where the anodic activity was initially localised on two electrodes, but later spread to a few neighbouring electrodes. The typical behaviour for this type of corrosion also included electrodes that remained anodic for several weeks, before slowly switching to cathodic activity, and electrodes where cathodic activity each week was predominantly concentrated near the most anodic electrodes. Although the damage remained fairly localised and evenly spread over about 5 electrodes, it was less localised than CEM I. A higher total porosity and lower pH value likely resulted in a larger surface area of steel being anodically activated due to increased number of connected paths for chloride penetration and steel depassivation. Similar behaviour was observed in our previous study [5]. The third type of corrosion behaviour, observed in CEM III and CEM IV, represented a combination of localised and general corrosion. Some electrodes remained heavily anodic over multiple weeks of exposure, while other electrodes were anodically activated during each wetting or drying cycle. The major difference between these two cements and previous two cements is the more refined pore structure (Fig. 1), which presumably distributed chlorides more evenly across the steel surface, resulting in less localised corrosion. CEM III in addition had the highest total porosity and the lowest pH value of the pore solution, making it the most susceptible to general corrosion, with the highest observed corrosion rates. Other authors [4] also linked higher porosity with higher corrosion rates, while percolation theory dictates that a decrease in total porosity results in the breakdown of the pore network into smaller, disconnected clusters, and this relation is extremely non-linear [20]. Even though CEM III exhibited the highest level of general corrosion, corrosion rates on individual electrodes also remained the highest throughout the 14-week exposure. At first glance, this is in contrast to observations in our previous study [5], where local corrosion rates in CEM I were the highest. However, the latter phenomenon only occurred after 30 weeks of exposure to chlorides, whereas CEM III showed the highest corrosion activity during the first 14 weeks. CMEA results are thus in agreement with our previous research [5], and provide additional information about the time evolution of these corrosion processes during the initial stages, including the degree of corrosion localization and the localised corrosion rates.

Similarly to measurements of electrochemical noise (EN) [34,54,55], the CMEA technique can distinctly measure the initiation times of corrosion, since metastable and transient corrosion events can be both detected and excluded from analysis. Looking at Figs. 4 to 7, the following initiation times can be determined for the various cements studied: 40 days (CEM I), 7 days (CEM II), 4 h (CEM III) and 4 days (CEM IV). The easiest way to explain these differences is by referring to the total porosities characterised previously [5]. It is known that a non-linear relationship exists between the total capillary porosity and the diffusion of oxygen and chloride ions, whereby a higher capillary porosity results in a higher rate of diffusion [20,56]. In this sense, it is reasonable that the CEM I cement, which had the lowest total porosity, also had the highest initiation time, while the CEM III cement, with the highest total porosity, had the lowest initiation time.

A typical wetting cycle incorporated a large peak in the corrosion rate at the very beginning of the wetting period. These high values were, thereafter, reduced to fairly low values before the drying period began, with the exception of in CEM I, where the reduction was slower. In a typical drying cycle, an evident peak in the corrosion rate appeared, with a certain delay, after the start of the drying period. This second peak was regularly lower than the peak at the beginning of wetting. The rise time and decrease in corrosion rate during drying was longest in CEM I and shortest in CEM IV. This behaviour can be explained by sufficient concentrations of oxygen and water at the steel surface, in combination with sufficient porosity, that enabled the necessary transport paths for either drying or saturation. The anodic and cathodic electrodes were not necessarily the same during the wetting and drying periods.

Some of the most important information provided by means of CMEA is the degree of corrosion localisation, and its evolution over time. Conventional electrochemical techniques, such as potentiodynamic scans (PD) and electrochemical impedance spectroscopy (EIS), measure certain corrosion parameters and then apply them equally cross the entire area of the polarized surface. If these parameters are localised on a smaller surface, an error is made [24,31]. Fig. 9 shows corrosion current densities on the most anodic electrode and the total corrosion current averaged across the entire exposed surface area. In Table 2 these two results are combined as a ratio between the localised current and the averaged current, defined as the corrosion localization index. Typical values for this index were around 10 or higher in our CMEA measurements. Additionally, the values for CEM II, CEM III and CEM IV appeared to reduce over time, indicating a transition towards more general corrosion. This was not the case in CEM I, where the index was, in fact, limited by the number of electrodes, and could be even higher provided that the array would contain >25 electrodes.

MicroCT volumes were scanned on all four specimens in order to validate the CMEA measurements, and both qualitative and quantitative analyses were performed. Although the CMEA and CT results were in good agreement for the majority of electrodes, a couple of electrodes exposed two potential pitfalls that should be taken into account when analysing CMEA measurements. The first is the problem of so-called self-corrosion, where anodic and cathodic locations occur on the same electrode. In such cases, only part of the corrosion current is measured through connection to a zero-resistance ammeter (ZRA). Examples of

Table 2

Corrosion localization indices for each specimen, calculated as the ratio between maximum local corrosion current densities (Fig. 9b) and average corrosion current densities (Fig. 9a) over a 3-week period.

	Week 1–3	Week 4–6	Week 7–9	Week 10–12	Week 13–14
CEM I	1.4	17.1	25.0	25.0	24.7
CEM II	19.5	19.2	11.7	10.9	9.0
CEM III	19.9	15.8	8.6	10.1	8.5
CEM IV	12.7	9.5	11.2	9.6	8.9

this are electrodes A2 and B3 in the CEM IV specimen (Fig. 10), where the corrosion damage estimated from the CT scan is evidently larger than that measured by the CMEA system. The second potential pitfall is the occurrence of crevice corrosion between an electrode and the protective epoxy resin. Electrodes A3 in CEM I and A2 in the CEM IV specimen provide potential examples of this, as corrosion is clearly visible along the length of the electrode. In theory, the appearance of crevice corrosion on an electrode would result in significant self-corrosion, but this is obviously not the case in general (cf., for example, the A3 electrode in CEM I). On the other hand, however, it is also questionable as to whether or not such crevices should be considered as completely uncharacteristic for steel corrosion in concrete. In reality, various types of steel joints and features can often represent an initiation site due to a poor interfacial transition zone (ITZ) [1], and the early corrosion mechanism may well be similar to crevice corrosion.

5. Conclusions

The coupled Multi-Electrode Array (CMEA) technique was successfully implemented to characterise the corrosion processes of steel in blended cement mortars, with 3 distinct corrosion behaviours observed: predominantly localised corrosion, localised corrosion that spread across a larger area over time, and a combination of localised and general corrosion. Results obtained by CMEA, in combination with microCT scans, provided a comprehensive insight into the time evolution of steel corrosion in these mortars, making it possible to form the following conclusions:

- It was established that a higher pH and lower total porosity (e.g. in CEM I) resulted in more localised corrosion, while cements with a higher porosity and lower pH (e.g., CEM III) exhibited a higher degree of general corrosion. Additionally, cements with lower porosity exhibited shorter corrosion initiation times compared to those with higher porosity.
- It was found that the general corrosion rate in cement CEM III reached fairly high values soon after the start of exposure, and remained stable after that. The general corrosion rates in cements CEM II and CEM IV started lower and increased after initiation, but remained below the corrosion rate in the CEM III cement.
- The corrosion localization index, denoted as the ratio between the maximum local corrosion rates at a single electrode, and the average corrosion rates over 25 electrodes, was highest in the CEM I cement, where only a single electrode was anodically active. In the CEM II and CEM III cements the localization index was higher at the beginning of the exposure, then diminished thereafter. The corrosion localization index was always relatively low (around 10) in the CEM IV cement. The maximum localised corrosion rates in cements CEM I, CEM II and CEM IV were comparable, and lower than those obtained in CEM III.
- Due to spatial information provided by the CMEA technique, more realistic corrosion rates were measured and, through summation, gave the actual corrosion damage. This was validated through qualitative and quantitative evaluation of microCT scans, which showed that CT and CMEA results were generally in good agreement. This indicated that the monitored corrosion behaviour was correct, and that only a few electrodes experienced self-corrosion.
- The highest corrosion rates were generated at the very beginning of the wetting periods. These corrosion rates rapidly diminished thereafter, except in the case of cement CEM I. The second corrosion rate peaks appeared soon after the start of the drying periods. The rise time and decrease in current fluctuation was longest in cement CEM I and shortest in CEM IV.
- The ability to also monitor the location and magnitude of cathodic reactions provided a comprehensive insight into how anodic locations are formed and maintained. It was found that corrosion activity on an electrode can pass from anodic to cathodic within a single wetting-drying cycle, depending on the saturation and drying ability of the mortar. This was especially valid for cements with more general corrosion.

Specific conclusions related to the various cements are in agreement with our previous study [5], in which the galvanostatic pulse (GP) technique and electrical resistance (ER) probes were applied. Only chlorides without accelerated carbonation were applied in the present research. In this sense, the extrapolation of outcomes to longer exposure periods, where carbonation cannot be excluded, might be misleading, and additional research is therefore required.

CRediT authorship contribution statement

Miha Hren: Conceptualization, Methodology, Validation, Investigation, Resources, Data curation, Writing – original draft, Visualization, Project administration, Funding acquisition. **Tadeja Kosec:** Conceptualization, Writing – review & editing, Supervision, Project administration. **Andraž Legat:** Conceptualization, Methodology, Writing – review & editing, Supervision, Project administration, Funding acquisition.

Declaration of competing interest

The authors declare the following financial interests/personal relationships which may be considered as potential competing interests: Miha Hren reports financial support was provided by Slovenian Research Agency (ARRS).

Data availability

Data will be made available on request.

Acknowledgements

The authors acknowledge financial support from the Slovenian Research Agency (research core funding No. P2-0273 and postdoc project No. Z2-2641).

The authors would also like to thank the Salonit Anhovo cement factory for providing the cements used in the research.

References

[1] U.M. Angst, M.R. Geiker, A. Michel, C. Gehlen, H. Wong, O.B. Isgor, B. Elsener, C. M. Hansson, R. François, K. Hornbostel, R. Polder, M.C. Alonso, M. Sanchez, M. J. Correia, M. Criado, A. Sagüés, N. Buenfeld, The steel–concrete interface, Mater. Struct. 50 (2017), https://doi.org/10.1617/s11527-017-1010-1.

[2] U.M. Angst, M.R. Geiker, M.C. Alonso, R. Polder, O.B. Isgor, B. Elsener, H. Wong, A. Michel, K. Hornbostel, C. Gehlen, R. François, M. Sanchez, M. Criado, H. Sørensen, C. Hansson, R. Pillai, S. Mundra, J. Gulikers, M. Raupach, J. Pacheco, A. Sagüés, The effect of the steel–concrete interface on chloride-induced corrosion initiation in concrete: a critical review by RILEM TC 262-SCI, Mater. Struct. 52 (2019) 88, https://doi.org/10.1617/s11527-019-1387-0.

[3] C.L. Page, Mechanism of corrosion protection in reinforced concrete marine structures, Nature 258 (1975) 514–515, https://doi.org/10.1038/258514a0.

[4] M. Stefanoni, U.M. Angst, B. Elsener, Kinetics of electrochemical dissolution of metals in porous media, Nat. Mater. 18 (2019) 942–947, https://doi.org/10.1038/s41563-019-0439-8.

[5] M. Hren, V. Bokan Bosiljkov, A. Legat, Effects of blended cements and carbonation on chloride-induced corrosion propagation, Cem. Concr. Res. 145 (2021), 106458, https://doi.org/10.1016/j.cemconres.2021.106458.

[6] M. Hren, T. Kosec, A. Legat, V. Bokan-Bosiljkov, Corrosion performance of steel in blended cement pore solutions, Mater. Technol. 53 (2019) 679–686, https://doi.org/10.17222/mit.2019.003.

[7] U. Angst, B. Elsener, C.K. Larsen, Ø. Vennesland, Critical chloride content in reinforced concrete - a review, Cem. Concr. Res. 39 (2009) 1122–1138, https://doi.org/10.1016/j.cemconres.2009.08.006.

[8] N. Gartner, T. Kosec, A. Legat, Monitoring the corrosion of steel in concrete exposed to a marine environment, Materials. 13 (2020) 407, https://doi.org/10.3390/ma13020407.

[9] O.E. Gjørv, Durability of reinforced concrete wharves in norwegian harbours, Matér. Constr. 2 (1969) 467–476, https://doi.org/10.1007/BF02478592.

[10] N.R. Jarrah, O.S.B. Al-Amoudi, M. Maslehuddin, O.A. Ashiru, A.I. Al-Mana, Electrochemical behaviour of steel in plain and blended cement concretes in

sulphate and/or chloride environments, Constr. Build. Mater. 9 (1995) 97–103, https://doi.org/10.1016/0950-0618(95)00002-W.

[11] D. Bjegovic, N. Stirmer, M. Serdar, Durability properties of concrete with blended cements, Mater. Corros. 63 (2012) 1087–1096, https://doi.org/10.1002/maco.201206699.

[12] T. Simčič, S. Pejovnik, G. De Schutter, V.B. Bosiljkov, Chloride ion penetration into fly ash modified concrete during wetting–drying cycles, Constr. Build. Mater. 93 (2015) 1216–1223, https://doi.org/10.1016/j.conbuildmat.2015.04.033.

[13] V.G. Papadakis, Effect of supplementary cementing materials on concrete resistance against carbonation and chloride ingress, Cem. Concr. Res. 30 (2000) 291–299, https://doi.org/10.1016/S0008-8846(99)00249-5.

[14] K.M.A. Hossain, M. Lachemi, Corrosion resistance and chloride diffusivity of volcanic ash blended cement mortar, Cem. Concr. Res. 34 (2004) 695–702, https://doi.org/10.1016/j.cemconres.2003.10.021.

[15] Q. Yuan, C. Shi, G. De Schutter, K. Audenaert, D. Deng, Chloride binding of cement-based materials subjected to external chloride environment – a review, Constr. Build. Mater. 23 (2009) 1–13, https://doi.org/10.1016/j.conbuildmat.2008.02.004.

[16] M.D.A. Thomas, R.D. Hooton, A. Scott, H. Zibara, The effect of supplementary cementitious materials on chloride binding in hardened cement paste, Cem. Concr. Res. 42 (2012) 1–7, https://doi.org/10.1016/j.cemconres.2011.01.001.

[17] M.V.A. Florea, H.J.H. Brouwers, Modelling of chloride binding related to hydration products in slag-blended cements, Constr. Build. Mater. 64 (2014) 421–430, https://doi.org/10.1016/j.conbuildmat.2014.04.038.

[18] P.-C. Aïtcin, Binders for Durable and Sustainable Concrete, CRC Press, London, 2008 (accessed July 8, 2016), http://nukweb.nuk.uni-lj.si/login?url=http://search.ebscohost.com/login.aspx?direct=true&db=nlebk&AN=201745&lang=sl&site=eds-live&scope=site.

[19] M. Stefanoni, U. Angst, B. Elsener, Corrosion rate of carbon steel in carbonated concrete – a critical review, Cem. Concr. Res. 103 (2018) 35–48, https://doi.org/10.1016/j.cemconres.2017.10.007.

[20] L. Bertolini, B. Elsener, P. Pedeferri, E. Redaelli, R.B. Polder, Corrosion of Steel in Concrete: Prevention, Diagnosis, Repair, Wiley-VCH Verlag GmbH & Co., Weinheim, Germany, 2013, https://doi.org/10.1002/9783527651696 (accessed July 8, 2016).

[21] E. McCafferty, Introduction to Corrosion Science, Springer, New York, 2010, https://doi.org/10.1007/978-1-4419-0455-3 (accessed July 8, 2016).

[22] S. Verma, S. Bhadauria, S. Akhtar, Monitoring corrosion of steel bars in reinforced concrete structures, Sci. World J. 2014 (2014) 1–9, https://doi.org/10.1155/2014/957904.

[23] G.S. Duffó, S.B. Farina, C.M. Giordano, Embeddable reference electrodes for corrosion monitoring of reinforced concrete structures, Mater. Corros. 61 (2010) 480–489, https://doi.org/10.1002/maco.200905346.

[24] B. Elsener, Corrosion rate of steel in concrete—Measurements beyond the tafel law, Corros. Sci. 47 (2005) 3019–3033, https://doi.org/10.1016/j.corsci.2005.06.021.

[25] M.F. Montemor, A.M.P. Simões, M.G.S. Ferreira, Chloride-induced corrosion on reinforcing steel: from the fundamentals to the monitoring techniques, Cem. Concr. Compos. 25 (2003) 491–502, https://doi.org/10.1016/S0958-9465(02)00089-6.

[26] L. Yan, G.-L. Song, Z. Wang, D. Zheng, Crevice corrosion of steel rebar in chloride-contaminated concrete, Constr. Build. Mater. 296 (2021), https://doi.org/10.1016/j.conbuildmat.2021.123587.

[27] N. Gartner, T. Kosec, A. Legat, Monitoring of the long-term performance of stainless steel reinforcement in saline environments, BHM Berg- Hüttenmänn. Monatshefte. 161 (2016) 44–49, https://doi.org/10.1007/s00501-016-0444-z.

[28] R.G. Duarte, A.S. Castela, R. Neves, L. Freire, M.F. Montemor, Corrosion behavior of stainless steel rebars embedded in concrete: an electrochemical impedance spectroscopy study, Electrochim. Acta 124 (2014) 218–224, https://doi.org/10.1016/j.electacta.2013.11.154.

[29] S.-J. Kwon, H.-S. Lee, S. Karthick, V. Saraswathy, H.-M. Yang, Long-term corrosion performance of blended cement concrete in the marine environment – a real-time study, Constr. Build. Mater. 154 (2017) 349–360, https://doi.org/10.1016/j.conbuildmat.2017.07.237.

[30] S. Qian, D. Qu, The influence of galvanic coupling on corrosion of carbon steel coupled with stainless steels for use in concrete structures, ECS Trans. 16 (2009) 127–140, https://doi.org/10.1149/1.3114954.

[31] U. Angst, M. Büchler, A new perspective on measuring the corrosion rate of localized corrosion, Mater. Corros. 71 (2020) 808–823, https://doi.org/10.1002/maco.201911467.

[32] J.P. Broomfield, K. Davies, K. Hladky, The use of permanent corrosion monitoring in new and existing reinforced concrete structures, Cem. Concr. Compos. 24 (2002) 27–34, https://doi.org/10.1016/S0958-9465(01)00024-5.

[33] W.J. McCarter, Ø. Vennesland, Sensor systems for use in reinforced concrete structures, Constr. Build. Mater. 18 (2004) 351–358, https://doi.org/10.1016/j.conbuildmat.2004.03.008.

[34] A. Legat, M. Leban, Ž. Bajt, Corrosion processes of steel in concrete characterized by means of electrochemical noise, Electrochim. Acta 49 (2004) 2741–2751, https://doi.org/10.1016/j.electacta.2004.01.036.

[35] A. Legat, Monitoring of steel corrosion in concrete by electrode arrays and electrical resistance probes, Electrochim. Acta 52 (2007) 7590–7598, https://doi.org/10.1016/j.electacta.2007.06.060.

[36] L. Yang, N. Sridhar, C.S. Brossia, D.S. Dunn, Evaluation of the coupled multielectrode array sensor as a real-time corrosion monitor, Corros. Sci. 47 (2005) 1794–1809, https://doi.org/10.1016/j.corsci.2004.08.002.

[37] P. Jakupi, J.J. Noël, D.W. Shoesmith, The evolution of crevice corrosion damage on the Ni–Cr–Mo–W alloy-22 determined by confocal laser scanning microscopy, Corros. Sci. 54 (2012) 260–269, https://doi.org/10.1016/j.corsci.2011.09.028.

[38] P. Jakupi, J.J. Noel, D.W. Shoesmith, Crevice corrosion initiation and propagation on Alloy-22 under galvanically-coupled and galvanostatic conditions, Corros. Sci. 53 (2011) 3122–3130, https://doi.org/10.1016/j.corsci.2011.05.061.

[39] A. Naganuma, K. Fushimi, K. Azumi, H. Habazaki, H. Konno, Application of the multichannel electrode method to monitoring of corrosion of steel in an artificial crevice, Corros. Sci. 52 (2010) 1179–1186, https://doi.org/10.1016/j.corsci.2010.01.005.

[40] F. Bocher, F. Presuel-Moreno, J.R. Scully, Investigation of crevice corrosion of AISI 316 stainless steel compared to Ni–Cr–Mo alloys using coupled multielectrode arrays, J. Electrochem. Soc. 155 (2008) C256–C268, https://doi.org/10.1149/1.2883741.

[41] N.D. Budiansky, J.L. Hudson, J.R. Scully, Origins of persistent interaction among localized corrosion sites on stainless steel, J. Electrochem. Soc. 151 (2004) B233, https://doi.org/10.1149/1.1666168.

[42] T.T. Lunt, V. Brusamarello, J.R. Scully, J.L. Hudsonb, Interactions among localized corrosion sites investigated with electrode arrays, Electrochem. Solid-State Lett. 3 (2000) 271, https://doi.org/10.1149/1.1391122.

[43] T. Kosec, M. Hren, A. Legat, Monitoring copper corrosion in bentonite by means of a coupled multi-electrode array, Corros. Eng. Sci. Technol. 52 (2017) 70–77, https://doi.org/10.1080/1478422X.2017.1312200.

[44] W. Wang, Y. Lu, Y. Zou, X. Zhang, J. Wang, The heterogeneous electrochemical characteristics of mild steel in the presence of local glucose oxidase—a study by the wire beam electrode method, Corros. Sci. 52 (2010) 810–816, https://doi.org/10.1016/j.corsci.2009.10.043.

[45] T.H. Muster, A.E. Hughes, S.A. Furman, T. Harvey, N. Sherman, S. Hardin, P. Corrigan, D. Lau, F.H. Scholes, P.A. White, M. Glenn, J. Mardel, S.J. Garcia, J.M. C. Mol, A rapid screening multi-electrode method for the evaluation of corrosion inhibitors, Electrochim. Acta 54 (2009) 3402–3411, https://doi.org/10.1016/j.electacta.2008.12.051.

[46] N.D. Budiansky, F. Bocher, H. Cong, M.F. Hurley, J.R. Scully, Use of coupled multi-electrode arrays to advance the understanding of selected corrosion phenomena, Corrosion 63 (2007) 537–554, https://doi.org/10.5006/1.3278405.

[47] A. Česen, T. Kosec, A. Legat, Characterization of steel corrosion in mortar by various electrochemical and physical techniques, Corros. Sci. 75 (2013) 47–57, https://doi.org/10.1016/j.corsci.2013.05.015.

[48] M. Hren, T. Kosec, A. Legat, Corrosion behavior of steel in pore solutions extracted from different blended cements, Mater. Corros. 71 (2020) 759–766, https://doi.org/10.1002/maco.202011548.

[49] EN 197-1:2011, Cement. Composition, Specifications and Conformity Criteria for Common Cements, 2011.

[50] EN 196-1:2016, Methods of Testing Cement. Determination of Strength, 2016.

[51] ASTM, ASTM G102-89: Standard Practice for Calculation of Corrosion Rates and Related Information from Electrochemical Measurements, 2016.

[52] M. Raupach, Chloride-induced macrocell corrosion of steel in concrete - theoretical background and practical consequences, Constr. Build. Mater. 10 (1996) 329–338, https://doi.org/10.1016/0950-0618(95)00018-6.

[53] A.A. Sagüés, M.A. Pech-Canul, A.K.M. Shahid Al-Mansur, Corrosion macrocell behavior of reinforcing steel in partially submerged concrete columns, Corros. Sci. 45 (2003) 7–32, https://doi.org/10.1016/S0010-938X(02)00087-2.

[54] A. Legat, V. Doleček, Chaotic analysis of electrochemical noise measured on stainless steel, J. Electrochem. Soc. 142 (1995) 1851, https://doi.org/10.1149/1.2044205.

[55] M. Leban, V. Doleček, A. Legat, Electrochemical noise during non-stationary corrosion processes, Mater. Corros. 52 (2001) 418–425, https://doi.org/10.1002/1521-4176(200106)52:6<418::AID-MACO418>3.0.CO;2-G.

[56] P.K. Mehta, P.J.M. Monteiro, Concrete: Microstructure, Properties, and Materials, McGraw-Hill, New York, 2006.